Stretchable Silver-Zinc Batteries Based on Embedded Nanowire Elastic Conductors

*Chaoyi Yan, Xu Wang, Mengqi Cui, Jiangxin Wang, Wenbin Kang, Ce Yao Foo, and Pooi See Lee**

Stretchable electronics represent a class of unconventional electronic devices based on soft substrates, in contrast to existing technology that is based on rigid substrates such as Si wafers.[1] Stretchable electronics can conform to complex non-planar surfaces, such as human organs, and provide unique functionalities. The soft form of electronics also allows the possibility to build up next-generation wearable and implantable electronics including health monitoring patches, hemispherical electronic eyes, smart clothes, and sensory skin.[2–6] One of the most challenging issues for the development of complete and independent stretchable system is the fabrication of stretchable power sources. Wireless coils were used to power several pioneer stretchable devices,[2,7] but it is highly desirable to develop stretchable forms of available power sources such as supercapacitors,[8–10] batteries,[7,11–14] and solar cells[15–17] to meet the imperative demands of stretchable, wearable, and implantable electronics.

Silver-zinc batteries, which are one of the most mature battery systems, hold promise as high-performance, safe, and green solutions to power stretchable devices. They have been widely used on a small scale such as in coin cells for watches and on a large scale for military and aerospace applications. Silver-zinc batteries have comparable specific energy to current market leader Li-ion batteries but can deliver much higher specific power. More importantly, silver-zinc batteries are inherently safe due to the use of water-based electrolytes and they are free from the flammability problems that have plagued the Li-ion batteries. They are also environmentally benign with the usage of non-toxic elements. The restricted application of silver-zinc battery in common consumer electronics such as laptops and cellphones is primarily due to the relatively high cost of silver. However, they are regaining interest as concerns over safety and environmental impact increase. For example, safety issue would become a larger consideration than cost when the batteries are used for wearable and implantable electronics. Moreover, they are promising candidates for applications in printed batteries for easy, low cost integration into future 2D and 3D printing processes for stretchable electronics due to their air stability, which is a key advantage compared to Li-ion batteries for printable device applications.

C. Y. Yan, X. Wang, M. Q. Cui, J. X. Wang, W. B. Kang, C. Y. Foo, Prof. P. S. Lee
School of Materials Science and Engineering
Nanyang Technological University
50 Nanyang Avenue, Singapore, 639798
E-mail: pslee@ntu.edu.sg

DOI: 10.1002/aenm.201301396

Here, we present the fabrication of silver-zinc battery based on stretchable Ag nanowire (AgNW) electrodes with embedded structures. The AgNW electrodes were fabricated via a lithographic filtration method and possess ideal bifunctionality by simultaneously providing electroactive materials and current collectors. The high-performance electrodes maintained their functions even when stretched up to 80% and are stable over 1000 cycles. Fully stretchable batteries are also demonstrated with both Ag and Zn electrodes and are stretchable. The full battery prototypes function properly in both relaxed and stretched states.

Schematic illustrations of the lithographic filtration method for stretchable AgNW electrode fabrication are shown in **Figure 1**a. Patterned filtration mask was prepared from cured polydimethylsiloxane (PDMS) substrate (thickness ≈ 1 mm), and they are used to selectively expose certain areas and obtain NW films with desired patterns, analogous to the role of ultraviolet (UV) masks in photolithography. AgNW dispersion (1 mg mL^{-1} in ethanol) was filtered to obtain very uniform NW films due to the simultaneous extraction of solvents from the evenly distributed holes in the track-etched polycarbonate (PC) membrane (Figure S1, Supporting Information). The thicknesses and hence resistances of the NW films can be controlled by the volume of NW dispersion added. Note that the soft PDMS mask was in intimate contact with the PC membrane due to the vacuum suction force and the sticky surface of PDMS, which is critical to prevent liquid spreading and obtain well-defined patterns. The PDMS mask was removed after filtration and then liquid PDMS was poured on top of the PC filter membrane with NW patterns. The liquid PDMS was cured and peeled off from the filter membrane. AgNW patterns were successfully transferred into the PDMS matrix and stretchable electrodes with embedded structures were obtained. Examples of the soft, stretchable AgNW electrodes are shown in Figure 1b (see also Figure S2, Supporting Information).

Structural characterizations of the stretchable AgNW electrodes are shown in **Figure 2**. The AgNWs embedded in PDMS elastomer matrix exhibit ideal bifunctionalities for battery applications by simultaneously providing electroactive layer and electron conducting layer. Because PDMS is not permeable to aqueous electrolyte,[18] only the surficial AgNW layer in contact with electrolyte (active layer) contributes to energy storage. Those AgNWs beneath the active layer serve as conducting layer to extract the electrons to external circuits. Scanning electron microscopy (SEM) characterizations of the AgNWs used can be found in Figure S3, Supporting Information. Figure 2b shows a top view of the AgNW/PDMS layer showing that the AgNWs are embedded in the elastomer matrix with part of the

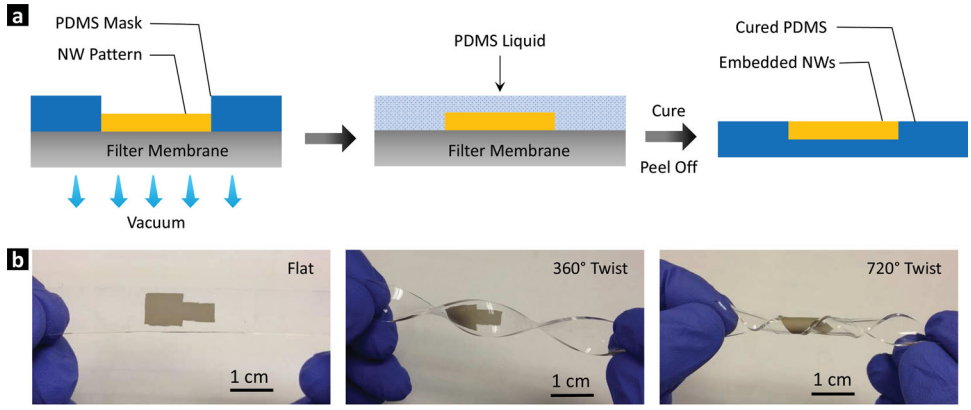

Figure 1. a) Illustrations of the lithographic filtration method to fabricate stretchable AgNW electrodes with embedded structures. b) Examples of the soft, stretchable electrodes in relaxed and twisted states.

NW surfaces exposed for electrochemical reactions. Note that instead of protruding from the surficial plane, all the NWs are lying flat within the top surface covering ≈10% to 15% of the surface area. A cross-sectional view of the stretchable electrode is shown in Figure 2c. The inset in Figure 2c shows an enlarged view of the cross-section, highlighting that the entire NW layer is fully embedded within the elastomer matrix. The electrodes showed excellent stretchability up to 100% without cracking or delaminating. Typical images of the electrode at 0% and 80% strain are shown in Figure 2d. The plot of resistance variations upon stretching and releasing is shown in Figure 2e. The electrode resistance gradually increased from 9.8 Ω (at 0% strain) to 15.4 Ω (at 100% strain) with an increase of 57% upon stretching and fully recovered upon releasing. The elastic conductor resistance changes upon stretching and releasing have been widely studied in previous reports.[5,19–21] Irreversible resistance changes were observed in the first several cycles (due to the irreversible NW sliding and rearrangements within the elastomer matrix) but the electrode resistance became fully recoverable after typically five cycles.[5,19–21] To rule out the possible effect of irreversible resistance change on battery performances, the AgNW electrodes were first stretched to 100% for 20 cycles before testing, and fully recoverable resistance change was observed (Figure 2e) for the cycled electrodes, which is consistent with previous findings. It is evident that the electrodes remain highly conductive even at 100% strain, ensuring their robust functioning at stretched states.

Electrochemical performances of the stretchable AgNW electrodes are shown in **Figure 3**. The electrodes were characterized using cyclic voltammetry (CV) and galvanostatic charge/discharge methods in a two-electrode system with a Zn plate as the counter and reference electrode (Figure S4, Supporting Information). CV curves of the electrode at 0% and 80% strains are compared in Figure 3a (scan rate 5 mV s^{-1}). The reversible cathodic reactions in silver-zinc battery are:[22]

$$2AgO + H_2O + 2e^- \leftrightarrow Ag_2O + 2OH^- \quad (1)$$

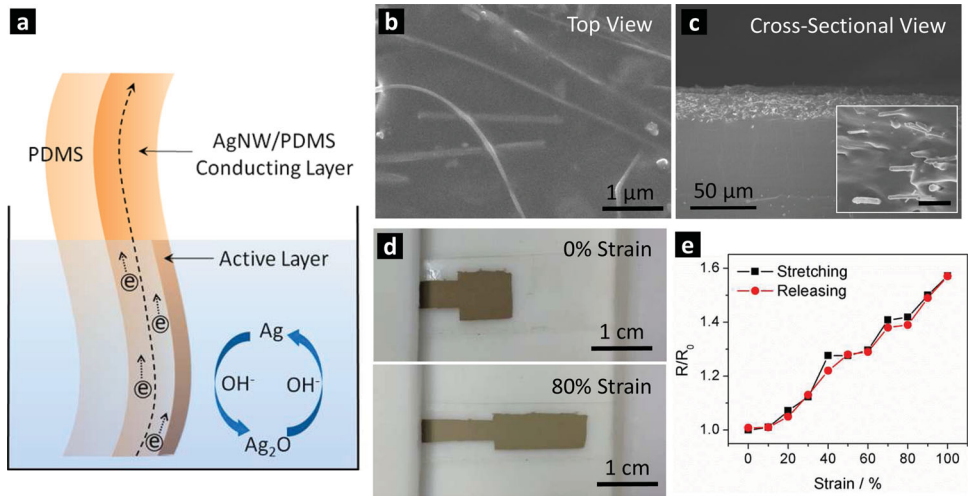

Figure 2. a) Schematic of the bi-functional stretchable AgNW electrode with embedded structure. b) Top view and c) cross-sectional view of the AgNWs embedded in PDMS matrix. The inset in (c) is an enlarged cross-sectional view. Scale bar: 2 µm. d) Stretching the electrode to 80% strain. e) Resistance change upon stretching and releasing of the electrode.

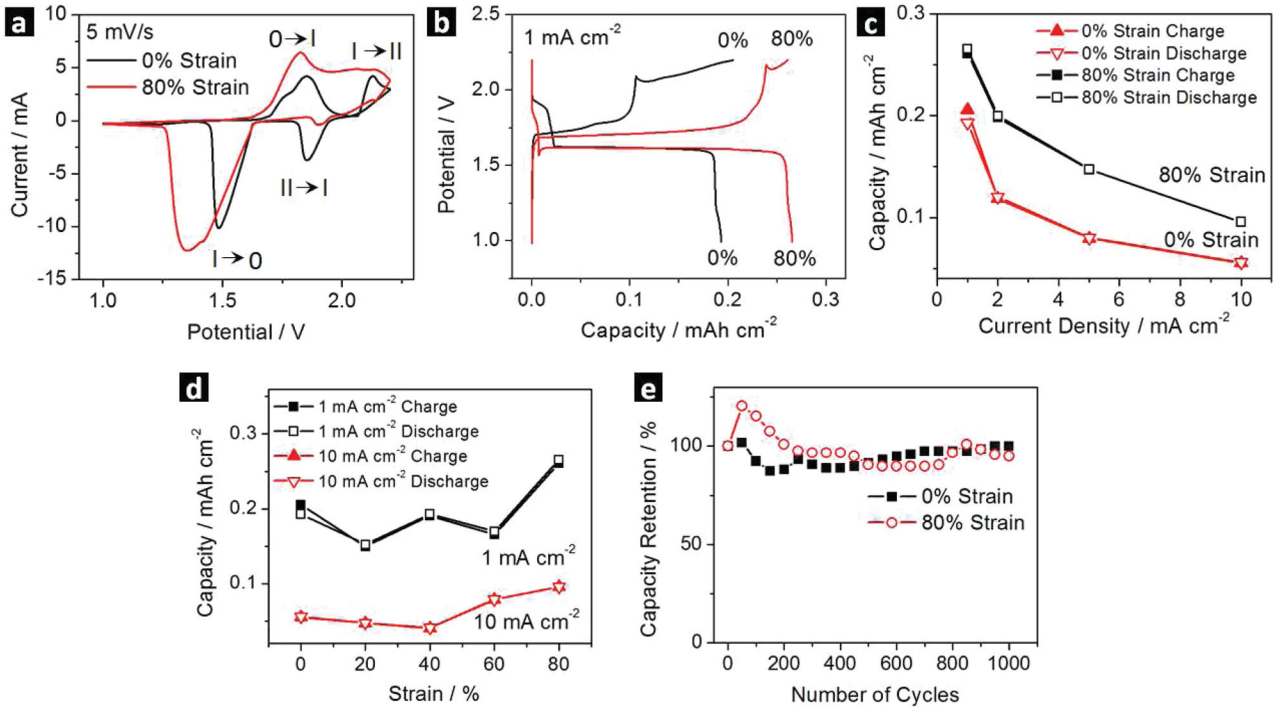

Figure 3. Electrochemical performances of the stretchable AgNW electrodes. a) CV curves at 0% and 80% strain (scan rate 5 mV s^{-1}). b) Charge/discharge curves at 0% and 80% strain (current density 1 mA cm^{-2}). The effect of c) charge/discharge current density and d) strain on electrode capacity. e) Cyclic stability of the stretchable electrodes at 0% and 80% strain.

$$Ag_2O + H_2O + 2e^- \leftrightarrow 2Ag + 2OH^- \quad (2)$$

Because elemental AgNWs were used for electrode fabrication, the NWs are oxidized first during the charging process and reduced when discharged. Oxidation conditions of the AgNWs, that is, whether they are fully or partially oxidized, depend on several parameters such as location of the NW within the embedded layer, NW diameters, and testing conditions (Figure S5, Supporting Information). At 0% strain (Figure 3a), two oxidation peaks were observed at 1.85 V (oxidation from Ag to Ag^+, 0 → I) and 2.13 V (oxidation from Ag^+ to Ag^{2+}, I → II), respectively. The corresponding reduction peaks appeared at 1.85 V (reduction from Ag^{2+} to Ag^+, II → I) and 1.48 V (reduction from Ag^+ to Ag, I → 0), respectively. When the electrode was stretched to 80%, the two sets of corresponding oxidation and reduction peaks could still be observed, with slight peak shifts from those at 0% strain. For example, the II → I reduction peak at 80% strain increased to 1.90 V from 1.85 V at 0% strain and the I → 0 reduction peak decreased to 1.35 V from 1.48 V at 0% strain. The relative peak shifts might originate from the larger electrode resistance in the stretched states (Figure 2e), which increases the electrochemical impedance and hence electrode polarizations.[22]

Charge/discharge curves at a current density of 1 mA cm^{-2} for electrodes at 0% and 80% strains are shown in Figure 3b. Analogous to those in the CV curves, two sets of charge/discharge potential plateaus are clearly visible for electrodes at both 0% and 80% strain, corresponding to the two-step oxidation/reduction reactions in Equations (1) and (2). The reversible reactions between Ag and monovalent Ag_2O (Equation (2), I ↔ 0) dominate the electrode capacity, as can also be viewed from CV curves (higher peaks for I ↔ 0 reactions). The 0 → I charge plateaus potential varied slightly with strain (Figure 3b), however, the I → 0 discharge plateaus potential remained identical at 1.62 V for both 0% and 80% strains. Detailed analyses for charge/discharge curves from 0% to 80% strains further verified that the stretchable battery electrodes showed ultrastable output voltage from 1.62–1.63 V (<1% fluctuations) independent of the stretching conditions (Figure S6, Supporting Information). This is of special importance for applications that require a stable voltage supply because no complex stretching-dependent voltage regulations are needed.

The dependence of areal capacity on charge/discharge current densities and strains are shown in Figure 3c,d, respectively. It is well-known that the capacity will decrease at higher current densities due to the less efficient utilization of active materials.[23,24] A degradation of 71% was obtained when the current density increased from 1 mA cm^{-2} to 10 mA cm^{-2} at 0% strain and the degradation is 64% for that at 80% strain (Figure 3b). Interestingly, the capacities at 80% strain are higher than those at 0% strain. At a fixed current density of 1 mA cm^{-2}, the areal capacity is 0.19 mAh cm^{-2} at 0% strain and increased to 0.27 mAh cm^{-2} at 80% strain. The relationship between areal capacity and strain is plotted in Figure 3d. The charge/discharge capacity is generally stable within small strains (0% to 60%), and increased slightly upon further stretching (60% to 80%), which may originate from the exposure of new NW surfaces when the electrodes are heavily stretched. With the unique embedded structure, only NWs in the surficial layer are active for electrochemical reactions. It is

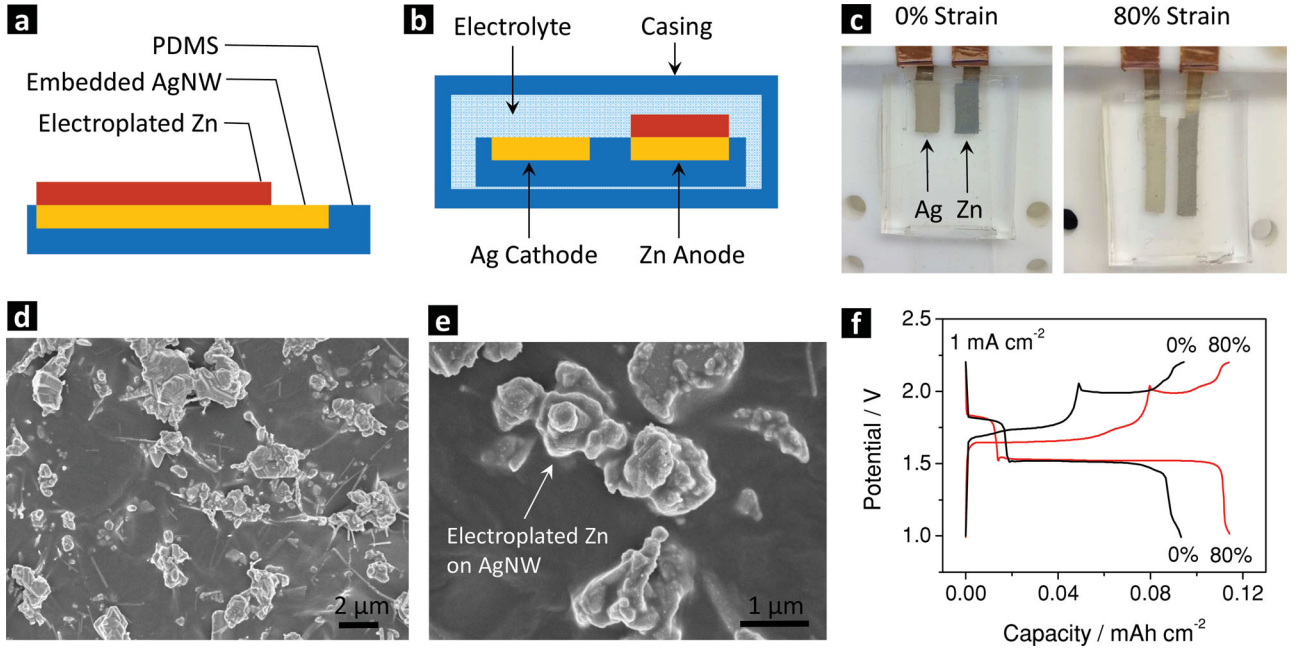

Figure 4. a,b) Cross-sectional schemes of the stretchable Zn electrode and full battery, respectively. Metallic Zn microstructures were deposited onto the stretchable AgNW electrodes via electroplating. c) Images of the stretchable full battery at 0% and 80% strain. The casing is not stretched in the setup. d,e) SEM images of the Zn microstructures on a AgNW electrode. f) Charge/discharge curves of the full battery at 0% and 80% strain.

difficult to determine the mass of the active NWs precisely, thus we use areal capacity (mAh cm^{-2}) instead of specific capacity (mAh g^{-1}) to characterize the stretchable electrodes. The maximum capacity we obtained is 0.27 mAh cm^{-2} (1 mA cm^{-2}, 80% strain), corresponding to an energy density of 0.44 mWh cm^{-2} (output voltage 1.62 V), which is comparable to previous reports with energy densities in the range of 0.01–4 mWh cm^{-2}.[25–27] For example, Dokko et al. reported the printing of Li-ion batteries with energy density of 0.01 mWh cm^{-2}.[25] Chamran et al. reported an energy density of 0.7 mWh cm^{-2} for 3D nickel-zinc alkaline microbatteries.[27] The energy density is lower than that for printed silver-zinc batteries[26] (≈4 mWh cm^{-2}) due to the much smaller active layer thickness and thus lower areal capacity. An reasonable estimation suggests that the thickness of the active layer for our stretchable electrode is ≈3–5 μm (Figure S7, Supporting Information), however, the Ag_2O layer thickness is >200 μm for the printed silver-zinc battery.[26] That is, with more than 40 times thinner materials, the energy density is only 9 times lower, revealing a much higher material utilization efficiency for our stretchable electrodes. The capacity of stretchable electrodes can be further improved by methods such as designing porous structures to increase the contact area of NWs with electrolytes.[11]

Cyclic stability of the stretchable AgNW electrode is shown in Figure 3e. The electrode can be cycled up to 1000 cycles (CV method, 50 mV s^{-1}) without obvious capacity degradation at both relaxed and stretched states (80% strain). The capacity fluctuations originate from the material activations and degradations, which have also been widely observed in previous reports.[28–30] This cyclic stability of our stretchable electrodes is comparable to or even better than state-of-the-art Li-ion batteries and silver-zinc batteries. We attribute the outstanding stability to the unique bifunctional electrode structures. The underlying AgNWs beneath the surficial active layer provide highly conductive and stable electron conducting paths for consistent energy output. Those AgNWs remain electrochemically inactive and are free from corrosion with electrolyte because PDMS does not allow aqueous solvents to infiltrate or swell the material.[18]

A complete battery in stretchable form was also demonstrated based on the successful development of stretchable AgNW electrodes. A stretchable Zn anode was fabricated by electroplating on AgNW/PDMS substrates. A schematic illustration of the stretchable Zn anode is shown in **Figure 4**a. SEM images of the Zn microstructures on the AgNW electrode is shown in Figure 4d,e. Zn particles with typical dimensions of several micrometers were deposited onto the exposed AgNW surface. Stretchable Ag and Zn electrodes with coplanar layout (Figure 4b) were used to assemble the full battery. Two AgNW electrodes were first fabricated on the same PDMS substrate, and then one of them was electroplated with Zn serving as anode. The single piece of substrate was placed in a PDMS casing filled with electrolyte (liquid electrolyte was used here for prototype demonstration and gel electrolyte may be developed for easy processing purpose). Example images of a full battery at 0% and 80% strain are shown in Figure 4c. The full battery exhibited similar charge/discharge behaviors (Figure 4f) as those for single AgNW electrode characterizations (Figure 3b). Areal capacities of 0.11 mAh cm^{-2} and 0.09 mAh cm^{-2} were observed for the full battery at 0% and 80% strain, respectively, which are lower than those achieved for AgNW electrodes probably due to the non-optimized Zn anode in the full battery prototype. While it is evident that the full battery prototype can function properly in the relaxed and stretched states, systematic

studies of the performance variations versus strain were hindered by the poor cyclic stability of Zn electrode. The Zn anode was quite reactive in alkaline electrolyte and we found that the Zn microstructures could only sustain tens of cycles before they were consumed (Figure S8, Supporting Information). The reaction of Zn with alkaline electrolyte and the associated gas evolution has been the most challenging issue for Ag-Zn battery system and has plagued their fabrication and application for decades. The Zn anodes are amalgamated with mercury to suppress the undesired reactions in commercial products.[31] Other anode additives such as lead (Pb) are also being investigated.[32] Although mercury-free Ag-Zn batteries were very recently developed by the Sony Corporation,[33] the successful suppression of hydrogen evolution requires complex material and device structural designs and might be pursued in detail in future studies.

In conclusion, we have demonstrated the successful fabrication of stretchable silver-zinc batteries based on embedded NW elastic conductors. Stretchable AgNW electrodes were fabricated using a lithographic filtration method. The electrodes possess ideal bifunctionalities by simultaneously providing electroactive materials and current collectors. Electrochemical performances of the AgNW electrodes were systematically studied in both the relaxed and stretched states and they maintained their functionalities, even when stretched up to 80%. The electrodes also showed outstanding cyclic stabilities without obvious performance degradation after 1000 cycles, which can be attributed to the unique embedded electrode structures. Fully stretchable batteries were also demonstrated with both Ag and Zn electrodes being stretchable. The Zn anode was fabricated by electroplating on AgNW electrodes. Notably, the full batteries can maintain their functionalities even in highly stretched states, although the cyclic stability needs to be improved in further studies. The innovative silver-zinc batteries in this stretchable form may find important applications in emerging stretchable and wearable electronics.

Experimental Section

Ag Electrode Fabrication: The PDMS mask is prepared from cured PDMS membrane (thickness ≈ 1 mm). The PDMS base and curer (Sylgard 184, Dow Corning) were mixed (weight ratio 10:1), degassed in a vacuum desiccator for 30 min to remove bubbles, cured at 60 °C for 2 h and then cut with graver to obtain the desired patterns. The soft mask was put on top of a PC filter membrane (Millipore GTTP, pore size 220 nm) for filtration. Commercially available AgNWs (Suzhou ColdStones Technology Co. Ltd., China) dispersed in ethanol (1 mg mL^{-1}) were used as received. The average diameter and length of the AgNWs were 40 nm and 50 µm, respectively. The AgNW dispersions were filtered and uniform NW patterns were obtained. The NW patterns were thoroughly rinsed with deionized (DI) water and clean ethanol to remove surfactants associated with NW synthesis processes. Liquid PDMS was poured on top of the filter membrane with NW patterns and then cured using the same procedure for mask fabrication. The solid PDMS membrane was peeled off from the PC membrane after curing and the NW patterns were successfully transferred to the PDMS elastomer matrix. The electrodes were used for testing without further treatments.

Zn Electrode Fabrication: Stretchable Zn electrodes were fabricated by electroplating on stretchable AgNW electrodes. A typical two-electrode setup was used for Zn electroplating, with Zn plate (purity > 99.9%) as counter and reference electrode and stretchable AgNW electrode as working electrode. Aqueous solution containing 1 M Zn_2SO_4 and 2 M KCl was used as electrolyte. Electroplating was performed at 1 mA cm^{-2} for 200 s using an electrochemical analyzer system (Autolab Potentiostat, PGSTAT302N).

Characterizations: Morphologies of the electrodes were characterized using SEM (JSM 7600F). The electrode was fixed on a customized optical stage to measure the resistance change upon stretching using Keithley source meter (Model: 2400). The electrode was then transferred to a home-built Teflon stage to apply desired strains for battery performance testing. Electrochemical properties of the electrodes were measured using a two-electrode system, with a Zn plate (purity > 99.9%) as the counter and reference electrode and 10 M aqueous NaOH as electrolyte in an electrochemical analyzer system (Autolab Potentiostat, PGSTAT302N).

Supporting Information

Supporting Information is available from the Wiley Online Library or from the author.

Acknowledgements

This work was supported in part by the Singapore National Research Foundation (CREATE Programme of Nanomaterials for Energy and Water Management). The authors thank M. F. Lin and X. W. Yan for their technical support and insightful discussions.

Received: September 12, 2013
Published online: October 29, 2013

[1] J. A. Rogers, T. Someya, Y. G. Huang, *Science* **2010**, *327*, 1603.
[2] D. H. Kim, N. S. Lu, R. Ma, Y. S. Kim, R. H. Kim, S. D. Wang, J. Wu, S. M. Won, H. Tao, A. Islam, K. J. Yu, T. I. Kim, R. Chowdhury, M. Ying, L. Z. Xu, M. Li, H. J. Chung, H. Keum, M. McCormick, P. Liu, Y. W. Zhang, F. G. Omenetto, Y. G. Huang, T. Coleman, J. A. Rogers, *Science* **2011**, *333*, 838.
[3] H. C. Ko, M. P. Stoykovich, J. Z. Song, V. Malyarchuk, W. M. Choi, C. J. Yu, J. B. Geddes, J. L. Xiao, S. D. Wang, Y. G. Huang, J. A. Rogers, *Nature* **2008**, *454*, 748.
[4] Y. M. Song, Y. Xie, V. Malyarchuk, J. Xiao, I. Jung, K.-J. Choi, Z. Liu, H. Park, C. Lu, R.-H. Kim, R. Li, K. B. Crozier, Y. Huang, J. A. Rogers, *Nature* **2013**, *497*, 95.
[5] D. J. Lipomi, M. Vosgueritchian, B. C. K. Tee, S. L. Hellstrom, J. A. Lee, C. H. Fox, Z. N. Bao, *Nat. Nanotechnol.* **2011**, *6*, 788.
[6] T. Yamada, Y. Hayamizu, Y. Yamamoto, Y. Yomogida, A. Izadi-Najafabadi, D. N. Futaba, K. Hata, *Nat. Nanotechnol.* **2011**, *6*, 296.
[7] S. Xu, Y. H. Zhang, J. Cho, J. Lee, X. Huang, L. Jia, J. A. Fan, Y. W. Su, J. Su, H. G. Zhang, H. Y. Cheng, B. W. Lu, C. J. Yu, C. Chuang, T. I. Kim, T. Song, K. Shigeta, S. Kang, C. Dagdeviren, I. Petrov, P. V. Braun, Y. G. Huang, U. Paik, J. A. Rogers, *Nat. Commun.* **2013**, *4*, 1543.
[8] L. B. Hu, M. Pasta, F. La Mantia, L. F. Cui, S. Jeong, H. D. Deshazer, J. W. Choi, S. M. Han, Y. Cui, *Nano Lett.* **2010**, *10*, 708.
[9] X. Li, T. L. Gu, B. Q. Wei, *Nano Lett.* **2012**, *12*, 6366.
[10] C. J. Yu, C. Masarapu, J. P. Rong, B. Q. Wei, H. Q. Jiang, *Adv. Mater.* **2009**, *21*, 4793.
[11] H. Lee, J. K. Yoo, J. H. Park, J. H. Kim, K. Kang, Y. S. Jung, *Adv. Energy Mater.* **2012**, *2*, 976.
[12] C. Y. Wang, W. Zheng, Z. L. Yue, C. O. Too, G. G. Wallace, *Adv. Mater.* **2011**, *23*, 3580.

[13] A. M. Gaikwad, A. M. Zamarayeva, J. Rousseau, H. W. Chu, I. Derin, D. A. Steingart, *Adv. Mater.* **2012**, *24*, 5071.
[14] M. Kaltenbrunner, G. Kettlgruber, C. Siket, R. Schwodiauer, S. Bauer, *Adv. Mater.* **2010**, *22*, 2065.
[15] J. Lee, J. A. Wu, M. X. Shi, J. Yoon, S. I. Park, M. Li, Z. J. Liu, Y. G. Huang, J. A. Rogers, *Adv. Mater.* **2011**, *23*, 986.
[16] M. Kaltenbrunner, M. S. White, E. D. Glowacki, T. Sekitani, T. Someya, N. S. Sariciftci, S. Bauer, *Nat. Commun.* **2012**, *3*, 770.
[17] D. J. Lipomi, B. C. K. Tee, M. Vosgueritchian, Z. N. Bao, *Adv. Mater.* **2011**, *23*, 1771.
[18] A. Mata, A. J. Fleischman, S. Roy, *Biomed. Microdevices* **2005**, *7*, 281.
[19] L. Cai, J. Li, P. Luan, H. Dong, D. Zhao, Q. Zhang, X. Zhang, M. Tu, Q. Zeng, W. Zhou, S. Xie, *Adv. Funct. Mater.* **2012**, *22*, 5238.
[20] F. Xu, X. Wang, Y. Zhu, Y. Zhu, *Adv. Funct. Mater.* **2012**, *22*, 1279.
[21] F. Xu, Y. Zhu, *Adv. Mater.* **2012**, *24*, 5117.
[22] J. Q. Pan, Y. Z. Sun, Z. H. Wang, P. Y. Wan, X. G. Liu, M. H. Fan, *J. Mater. Chem.* **2007**, *17*, 4820.
[23] H. Jiang, T. Zhao, J. Ma, C. Y. Yan, C. Z. Li, *Chem. Commun.* **2011**, *47*, 1264.
[24] C. Y. Yan, H. Jiang, T. Zhao, C. Z. Li, J. Ma, P. S. Lee, *J. Mater. Chem.* **2011**, *21*, 10482.
[25] K. Dokko, J. Sugaya, H. Nakano, T. Yasukawa, T. Matsue, K. Kanamura, *Electrochem. Commun.* **2007**, *9*, 857.
[26] K. T. Braam, S. K. Volkman, V. Subramanian, *J. Power Sources* **2012**, *199*, 367.
[27] F. Chamran, H. S. Min, B. Dunn, C. J. Kim, *MEMS 2006: 19th IEEE Int. Conf. Micro Electro Mech. Syst.* **2006**, 950.
[28] L.-F. Cui, Y. Yang, C.-M. Hsu, Y. Cui, *Nano Lett.* **2009**, *9*, 3370.
[29] A. Magasinski, P. Dixon, B. Hertzberg, A. Kvit, J. Ayala, G. Yushin, *Nat. Mater.* **2010**, *9*, 353.
[30] P. L. Taberna, S. Mitra, P. Poizot, P. Simon, J. M. Tarascon, *Nat. Mater.* **2006**, *5*, 567.
[31] J. Kwasnik, H. Lapinski, *J. Power Sources* **1982**, *8*, 67.
[32] D. F. Smith, J. A. Gucinski, *J. Power Sources* **1999**, *80*, 66.
[33] T. Ohhara, S. Sato, Sony Corporation, **2003**, Patent Number: *EP1505668 B1*.